Protein Science (1997), 6:355–363. Cambridge University Press. Printed in the USA.

Backbone and side-chain dynamics of residues in a partially folded β-sheet peptide from platelet factor-4

VLADIMIR A. DARAGAN, ELENA E. ILYINA, CYNTHIA G. FIELDS, GREGG B. FIELDS, AND KEVIN H. MAYO

Department of Biochemistry, Biomedical Engineering Center, University of Minnesota, 420 Delaware Street, S.E., Minneapolis, Minnesota 55455

(RECEIVED July 23, 1996; ACCEPTED November 13, 1996)

Abstract

Structurally characterizing partially folded states is problematic given the nature of these transient species. A peptide 20mer, T_{38}AQLIATLKNGRKISLDLQA$_{57}$ (P20), which has been shown to partially fold in a relatively stable turn/loop conformation (LKNGR) and transient β-sheet structure, is a good model for studying backbone and side-chain mobilities in a transiently folded peptide by using ^{13}C-NMR relaxation. Here, four residues in P20, A43, T44, G48, and I51, chosen for their positions in or near the loop conformation and for compositional variety, have been selectively ^{13}C-enriched. Proton-coupled and decoupled ^{13}C-NMR relaxation experiments have been performed to obtain the temperature dependencies (278 K to 343 K) of auto- and cross-correlation motional order parameters and correlation times. In order to differentiate sequence–neighbor effects from folding effects, two shorter peptides derived from P20, IATLK (P5) and NGRKIS (P6), were similarly ^{13}C-enriched and investigated. For A43, T44, G48, and I51 residues in P20 relative to those in P5/P6, several observations are consistent with partial folding in P20: (1) $C_\alpha H$ motional tendencies are all about the same, vary less with temperature, and are relatively more restricted, (2) G48 $C_\alpha H_2$ $\phi(t)$, $\psi(t)$ rotations are more correlated, and (3) methyl group rotations are slower and yield lower activation energies consistent with formation of hydrophobic "pockets." In addition, T44 and I51 $C_\beta H$ mobilities in P20 are more restricted at lower temperature than those of their $C_\alpha H$ and display significantly greater sensitivity to temperature suggesting a larger enthalpic contribution to side-chain mobility. Moreover, at higher temperatures, side-chain methyls and methylenes in P20 are more motionally restricted than those in P5/P6, suggesting that some type of "folded" or "collapsed" structure remains in P20 for what normally would be considered an "unfolded" state.

Keywords: β-sheet; dynamics; NMR; peptide; relaxation

Structurally characterizing partially folded proteins and peptides is an area of interest in the protein folding field, but has been problematic given the transient nature of these species. When the structural distribution is broad and the lifetime of a conformation is sub-milliseconds, ^{1}H-^{1}H NOEs are weak and have insufficient time to develop, and J-coupling constants and chemical shifts average becoming conformationally uninformative. In this case, the normally employed NMR solution structure approach fails. Although most solution NMR studies have been focused on biomolecular structure, ^{13}C and ^{15}N NMR relaxation measurements also can produce a wealth of information about internal rotations and correlated motions in proteins and peptides via analysis of various auto- and cross-correlation spectral density functions, e.g., $J_{ab}(\omega)$, using an appropriate motional model. Spectral density functions derived from ^{13}C NMR relaxation measurements are sensitive to events like the motions of backbone and side-chain CH and NH bonds, which occur on the nanosecond to picosecond time scale. Internal motional differences of a given residue in a partially folded state compared to that same residue in a solvent-exposed "non-folded" or "less folded" state may be detected by analyzing and comparing ^{13}C and ^{15}N NMR relaxation data from both states.

Most ^{13}C and ^{15}N NMR relaxation measurements aimed at studying protein/peptide motional dynamics have been performed using proton-decoupling that yields auto-correlation spectral densities and, from these, the generally well known auto-correlation times and order parameters. Additional, and often more informative, motional parameters can be derived from proton-coupled ^{13}C NMR multiplet relaxation experiments that provide cross-correlation spectral densities, e.g., $J_{HCH}(\omega)$, describing motions of a pair of geometrically related CH-bond vectors in methylene and methyl groups (Daragan et al., 1974; Bain & Lynden-Bell, 1975; Werbelow & Grant, 1977; Vold & Vold, 1978; Canet, 1989; Grant et al., 1991; Kumar & Madhu, 1996). This term is more sensitive to motional

Reprint request to: Kevin H. Mayo, Department of Biochemistry, Biomedical Engineering Center, University of Minnesota, 420 Delaware Street, S.E., Minneapolis, MN 55455.

Abbreviations: NMR, nuclear magnetic resonance; 2D NMR, two-dimensional NMR spectroscopy; NOE, nuclear Overhauser effect; rf, radio frequency; FID, free induction decay; PF4, platelet factor-4.

anisotropy. Spectral densities are most commonly analyzed by using a model-free approach (Lipari & Szabo, 1982a, 1982b; Peng & Wagner, 1995) or some other rotational model (Daragan & Mayo, 1993, and references therein; Daragan et al., 1993). Spectral density mapping (Peng & Wagner, 1992, 1994) also can provide additional information about the shape of the spectral density function, which reflects the distribution of frequencies of motional vectors. This more involved approach, however, is usually unnecessary since these distributions can be described relatively well by using the simple Lipari-Szabo model free approach (Lipari & Szabo, 1982a, 1982b; Peng & Wagner, 1995) where a bond rotation is considered to be the combination of two processes: isotropic overall molecular tumbling and some internal rotation defined by a single exponential correlation function. Although more complicated descriptions can be constructed to account for two or more internal motions (Clore et al., 1990), such analyses are limited by the accuracy of the NMR relaxation data. The most reliable information obtained from these analyses, therefore, is the motional order parameter, S^2 (Lipari & Szabo, 1982a, 1982b), which is related to the degree of motional restriction at a particular nucleus. S^2 is the limiting value of a respective auto- or cross-correlation function. For NH, CH methines, and proton-decoupled ^{13}C relaxation for CH_2 and CH_3 groups, only auto-correlation order parameters can be obtained accurately. For methyl and methylene groups, however, proton-coupled ^{13}C relaxation spectra allow derivation of a cross-correlation order parameter, S^2_{ab}, which can be defined from cross-correlation functions of rotations of two different, but geometrically-related, motional vectors, $\boldsymbol{a}$ and $\boldsymbol{b}$, directed along CH or HH bonds (Kay & Torchia, 1991; Daragan & Mayo, 1995; Zhu et al., 1995). The relationships between various auto- and cross-correlation order parameters can provide very useful information about the geometric characteristics of rotations, i.e., the direction of the effective axis of rotation in the molecular frame, rotational restrictions, shape of the potential well within which multiple rotations occur, and so on (Daragan & Mayo, 1995, 1996a, 1996b; Zhu et al., 1995).

Although some motional dynamics studies have been aimed at understanding protein/peptide side-chain motions (Dellwo & Wand, 1989; Weaver et al., 1989; Palmer et al., 1991; Nicholson et al., 1992; Stone et al., 1993; Bremi et al., 1994; Jarvis & Craik, 1995; Mikhailov et al., 1995a,b; Mispelter et al., 1995; Zhu et al., 1995), most have been focused on $^{13}C_\alpha H$ and ^{15}NH backbone motions (e.g., Clore & Gronenborn, 1993; Peng & Wagner, 1994). In the present study, ^{13}C NMR relaxation experiments are focused on studying side-chain and backbone internal motions of residues in a partially folded peptide derived from platelet factor-4 (PF4) (Ilyina et al., 1994). This peptide (P20) is twenty residues in length (Fig. 1, bottom). Between 5 °C and 10 °C, numerous conformationally constraining ^1H NOEs were observed within the sequence L45 to R49 (Ilyina et al., 1994). Distance geometry calculations using these NOE constraints demonstrated that P20 forms a native-like turn/loop conformation (L45 to R49) that is probably stabilized by formation of a transient β-sheet (Ilyina et al., 1994). A small ensemble of these structures superimposed is shown in Figure 1. Note the relatively well defined turn/loop and the structurally undefined strands. At temperatures above about 15 °C, even the turn/loop NOEs are not observed indicating dimished populations of this turn conformation.

Here, synthetic peptide P20 has been selectively ^{13}C-enriched in four residues: A43, T44, G48, and I51. These particular residues were chosen for study due to their positions near the turn/loop

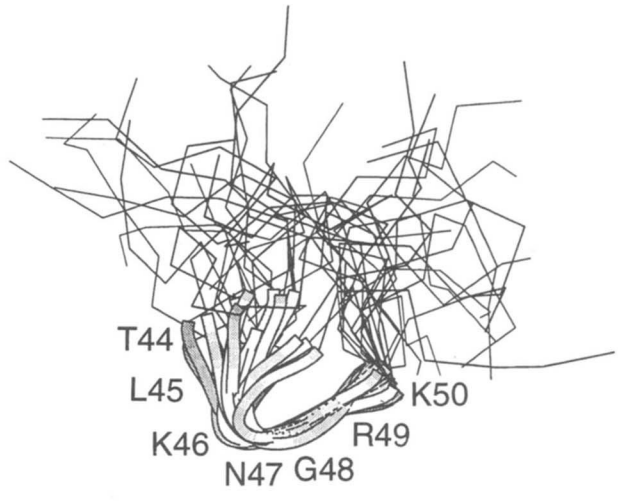

Fig. 1. The amino acid sequence for P20 is given at the bottom of this figure using the single letter code. The numbering for amino acid residues in P20 (38–57) is the same at that used for parent platelet factor-4 (PF4) (Ilyina et al., 1994). Twenty distance geometry calculated structures are overlaid above the sequence to show the general folding of this peptide derived by using NOE distance constraints acquired at 278 K. Structures were taken from Ilyina et al. (1994).

conformation. G48 is part of the turn/loop (Fig. 1) and provides an excellent motional probe via analysis of $^{13}CH_2$ cross-correlation spectral densities, which are more sensitive to motional anisotropy than standard auto-correlation functions. A43 and I51 have hydrophobic side chains and are paired across strands in the β-sheet in native PF4 and possibly in partially folded P20. Moreover, A43 provides a simple methyl group as its side chain, while I51 provides the full variety of methine, methylene, and methyl groups. The isoleucine side chain is also expected to demonstrate increased motional restrictions due to its bulky nature. T44 was included in this study due to its preponderance in β-sheet structures and its position in the turn/loop region. To differentiate sequence–neighbor effects from folding effects in P20, shorter penta- and hexapeptides (P5 and P6 identified in Figure 1) derived from the same sequence have been investigated as well. From proton-coupled and decoupled ^{13}C NMR relaxation measurements, auto- and cross-correlation spectral densities have been determined and have been analyzed by using the model-free approach. Furthermore, since partial structure in P20 appears at lower temperatures, the temperature dependence of motional parameters was investigated. Observation of relatively restricted motions in P20 at higher temperatures may indicate the presence of at least partially collapsed states.

Theory

In the model-free approach parameterized with a single internal correlation time, spectral densities for motional vectors $\boldsymbol{a}$ and $\boldsymbol{b}$ can be written as (Lipari & Szabo, 1982a; Kay & Torchia, 1991; Daragan & Mayo, 1995; Zhu et al., 1995):

$$J_{ab}(\omega) = S_{ab}^2\tau_o/(1 + \omega^2\tau_o^2) + [P_2(\cos\theta_{ab}) - S_{ab}^2]\tau_i'/(1 + \omega^2\tau_i'^2) \quad (1)$$

where $\tau_i' = \tau_o\tau_i/(\tau_o + \tau_i)$. τ_o and τ_i are correlation times for overall tumbling and internal rotations, respectively. $P_2(x) = 0.5(3x^2 - 1)$ is the second order Legendre polynomial, and θ_{ab} is the angle between vectors $\boldsymbol{a}$ and $\boldsymbol{b}$. The order parameter S_{ab}^2 can be defined for both auto- and cross-correlation spectral densities as:

$$S_{ab}^2 = \frac{4\pi}{5}\sum_{m=-2}^{2}\langle Y_{2m}(\theta_a, \phi_a)\rangle\langle Y_{2m}^*(\theta_b, \phi_b)\rangle \quad (2)$$

where Y_{2m} is the second order spherical harmonics; θ_a and ϕ_a are the polar angles for bond vector $\boldsymbol{a}$ in the molecular frame. Averaging is performed over all allowed orientations of $\boldsymbol{a}$ and $\boldsymbol{b}$. If $\boldsymbol{a} = \boldsymbol{b}$, S_{ab}^2 is the auto-correlation order parameter, and when $\boldsymbol{a} \neq \boldsymbol{b}$, S_{ab}^2 is the cross-correlation order parameter. For the methylene group, one can determine CH bond motional auto- and cross-correlation order parameters S_{CH}^2 and S_{HCH}^2 (same as $S_{CH'CH}^2$) from proton-coupled ^{13}C multiplet NMR relaxation measurements (Kay & Torchia, 1991; Daragan & Mayo, 1995; Zhu et al., 1995). Moreover, since different relationships exist between S_{CH}^2 and S_{HCH}^2 for different rotational models, knowing these relationships allows one to discriminate among various models. Many of these relationships have been defined by Daragan and Mayo (1995).

If two internal rotations, ω_1 and ω_2, determine motions of a methylene group, e.g., ϕ and ψ backbone rotations for glycine, correlation of these rotations can be studied by determining S_{CH}^2 and S_{HCH}^2 (Daragan & Mayo, 1996b). For two restricted internal rotations:

$$S_{HCH}^2 = 1/6 - (1/2)S_{CH}^2 - (10/9)R_1R_2c_{12} \quad (3)$$

where R_1 and R_2 are the amplitudes of the restricted rotations and the rotational correlation coefficient $-1 \leq c_{12} \leq 1$. By experimentally determining S_{CH}^2 and S_{HCH}^2, the sign of the rotational correlation coefficient can be derived by using Equation 3. For uncorrelated motions, i.e., $c_{12} = 0$, the relationship between S_{CH}^2 and S_{HCH}^2 is exactly the same as that for rotation about a single axis (Daragan & Mayo, 1995). In the limit of fully correlated ($c_{12} = 1$) or anti-correlated ($c_{12} = -1$) rotations, motions of the CH_2 group can be considered rotations about a single effective axis. For anti-correlated rotations of equal amplitude, i.e., $R_1 = R_2$, this axis is directed perpendicular to the HCH plane, while for fully correlated rotations, this axis bisects the HCH angle (Daragan & Mayo, 1996b).

For N correlated, low amplitude (<1 rad) restricted rotations, the auto-correlation order parameter for motional vector $\boldsymbol{a}$ can be written as (Daragan & Mayo, 1996b):

$$S_a^2 = 1 - \frac{3}{2}\sum_{k,l=1}^{N}(\cos\theta_{kl} - \cos\theta_{kA}\cos\theta_{lA})R_kR_lc_{kl} \quad (4)$$

where θ_{kl} is the angle between the two rotational axes, k and l, and θ_{kA} is the angle between vector $\boldsymbol{A} = \langle\boldsymbol{a}(t)\rangle$ and rotational axis k. The averaging $\langle\boldsymbol{a}(t)\rangle$ should be performed in the molecular coordinate system. As an example, consider motions of $C_\alpha H$ and $C_\beta H$ bond vectors. If one assumes that $C_\alpha H$ bond motions are primarily determined by ϕ,ψ rotations, while $C_\beta H$ bond motions are primarily determined by ϕ,ψ, and χ_1 rotations, Equation 4 can be used to obtain:

$$S_\alpha^2 = 1 - \tfrac{3}{2}[\sin^2\theta_{\alpha\phi}R_\phi^2 + \sin^2\theta_{\alpha\psi}R_\psi^2 + 2(\cos\theta_{\phi\psi} - \cos\theta_{\alpha\phi}\cos\theta_{\alpha\psi})R_\phi R_\psi c_{\phi\psi}] \quad (5a)$$

$$S_\beta^2 = 1 - \tfrac{3}{2}(\sin^2\theta_{\beta\phi}R_\phi^2 + \sin^2\theta_{\beta\psi}R_\psi^2 + \sin^2\theta_{\beta\chi}R_\chi^2) - 3(\cos\theta_{\phi\psi} - \cos\theta_{\beta\phi}\cos\theta_{\beta\psi})R_\phi R_\psi c_{\phi\psi} - 3(\cos\theta_{\phi\chi} - \cos\theta_{\beta\phi}\cos\theta_{\beta\chi})R_\phi R_\chi c_{\phi\chi} - 3(\cos\theta_{\psi\chi} - \cos\theta_{\beta\psi}\cos\theta_{\beta\chi})R_\psi R_\chi c_{\psi\chi}. \quad (5b)$$

To better understand the influence of various rotational correlations on motional order parameters, S_α^2 and S_β^2 have been calculated for peptide geometries obtained with the program DISCOVER (Version 3.1; Biosym Technologies, Inc.). Simulations were performed for standard peptide conformations: α-helix, β-sheet, and extended chain. Using an isoleucine residue as an example, the equilibrium value for the χ_1 angle, χ_{1e}, in any of these conformations was about +60°. Therefore, this isoleucine χ_{1e} value will be used in the following examples. The cosines of angles in equations 5a and b have been calculated as: $\cos\theta_{\phi\psi} = -0.358$; $\cos\theta_{\phi\chi} = 0.364$; $\cos\theta_{\psi\chi} = 0.372$; $\cos\theta_{\alpha\phi} = 0.302$; $\cos\theta_{\alpha\psi} = 0.284$; $\cos\theta_{\alpha\chi} = -0.314$; $\cos\theta_{\beta\phi} = -0.262$; $\cos\theta_{\beta\psi} = -0.351$; $\cos\theta_{\beta\chi} = 0.286$. It should be emphasized that only $\theta_{\beta\phi}$ and $\theta_{\beta\psi}$ changed with different values of χ_{1e}. Results of these calculations have been plotted in Figure 2 as S_β^2/S_α^2 versus the rotational correlation coefficient $c_{\phi\psi}$.

For uncorrelated $\phi(t)$, $\psi(t)$, $\chi_1(t)$ rotations, i.e., when $c_{\phi\psi} = c_{\chi\phi} = c_{\chi\psi} = 0$, S_β^2 is less than S_α^2 for $\chi_{1e} = 60°$. However, for very low amplitude χ rotations, S_β^2 can be greater than S_α^2. S_β^2 also can be greater than S_α^2 when internal rotations are correlated. Negatively correlated $\phi(t)$, $\psi(t)$ rotations and positively correlated $\phi(t)$,

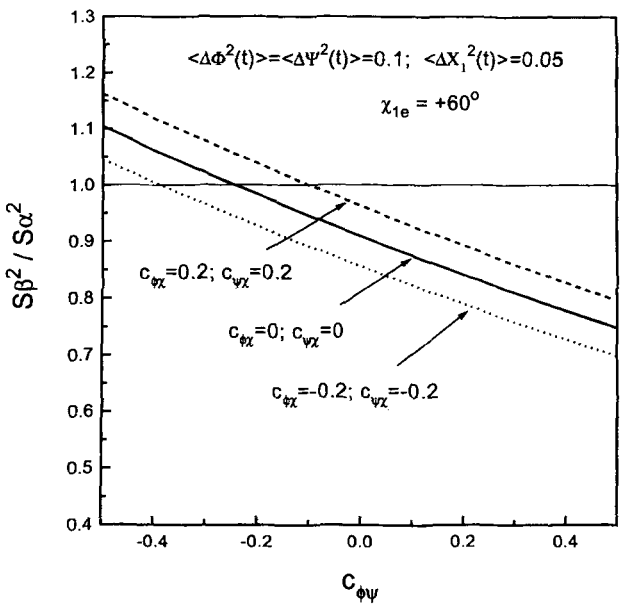

Fig. 2. The calculated ratio of auto-correlation order parameters for $C_\beta H$ and $C_\alpha H$ bonds in a polypeptide is shown for different values of rotational correlation coefficients as described in the text. Bond rotations were assumed to be mainly determined by $\phi(t)$, $\psi(t)$ and $\chi_1(t)$ rotations.

$\chi(t)$ and $\psi(t)$, $\chi(t)$ rotations can restrict $C_\beta H$ motions leading to $S_\beta^2 > S_\alpha^2$. Previously, it was shown (Daragan & Mayo, 1996b) that for α-helix structure, $c_{\phi\psi} < 0$ making $S_\beta^2 > S_\alpha^2$ highly probable, while for a β-strand conformation, $c_{\phi\psi} \geq 0$ making the opposite, i.e., $S_\beta^2 < S_\alpha^2$, more probable. In real peptides and proteins, the relationships between S_β^2 and S_α^2 can of course be modified by other internal rotations which were not considered in this simple model. Nevertheless, this exercise is useful in helping to understand the connection between rotational correlation coefficients and experimentally determined NMR relaxation parameters.

Since methyl group rotations are unrestricted, a different approach should be applied to analyzing their ^{13}C relaxation data. The Lipari-Szabo model free approach parameterized with two internal correlation times (Kay & Torchia, 1991; Daragan & Mayo, 1996a) approximates, fairly reasonably, many types of methyl group rotations. For tetrahedral methyl group geometry, auto- and cross-correlation order parameters can be related as:

$$S_{CH}^2 = S_{HCH}^2 = S_o^2/9 \quad (6)$$

where S_o^2 is the order parameter for overall tumbling of the methyl group symmetry axis. For a more detailed description of methyl motions, one can use the method of Clore et al. (Clore et al., 1990; Kay & Torchia, 1991; Daragan & Mayo, 1996a), which considers two internal correlation times. Applications of this method for calculating auto- and cross-correlation spectral densities have been described by Kay & Torchia (1991) and by Daragan & Mayo (1996a). However, for approximating internal correlation times, the standard Lipari- Szabo model-free approach is generally sufficient. Sometimes it is useful to calculate the spectral density $J_Z(\omega)$ or the correlation time $\tau_Z = J_Z(0)$ of the methyl group symmetry axis from NMR relaxation data. Daragan and Mayo (1996a) showed that for any motional model applied to tetrahedral methyl group rotations, one can write:

$$J_Z(\omega) = 3[J_{CH}(\omega) + 2J_{HCH}(\omega)]. \quad (7)$$

Results and discussion

For P20, T_{38}AQLIATLKNGRKISLDLQA$_{57}$ (Fig. 1), A43, T44, G48, and I51 have been ^{13}C-enriched in backbone and side-chain carbon positions. The numbering of amino acid residues in the sequence is the same as in parent PF4 (Ilyina et al., 1994). The temperature dependencies of proton-decoupled ^{13}C spin-lattice relaxation rates, W, were measured at two NMR frequencies (150 and 62.5 MHz). In addition, heteronuclear $\{^1H\}$-^{13}C NOEs and ^{13}C-multiplet (proton-coupled) spin-lattice relaxation rates for outer and inner multiplet lines, W_o, W_i, respectively, were also measured at a ^{13}C NMR frequency of 150 MHz. In order to differentiate motions not directly resulting from P20 folding, short "control" peptides derived from the P20 sequence, I_{52}ATLK$_{56}$ (P5) and N_{47}GRKIS$_{52}$ (P6), and ^{13}C enriched in the same amino acid residues were similarly investigated. Typical $^{13}C_\alpha$ relaxation data are exemplified in Figures 3 and 4 for G48 (Fig. 3) and for T44 and I51 (Fig. 4) in P20 and P6. For P20, and even for the short hexapeptide P6, G48 ^{13}C spin-lattice relaxation rates acquired at the two resonance frequencies (Fig. 3) differ significantly, indicating that overall motions are not at the extreme narrowing limit. In this respect, the frequency dependence of relaxation rates provides

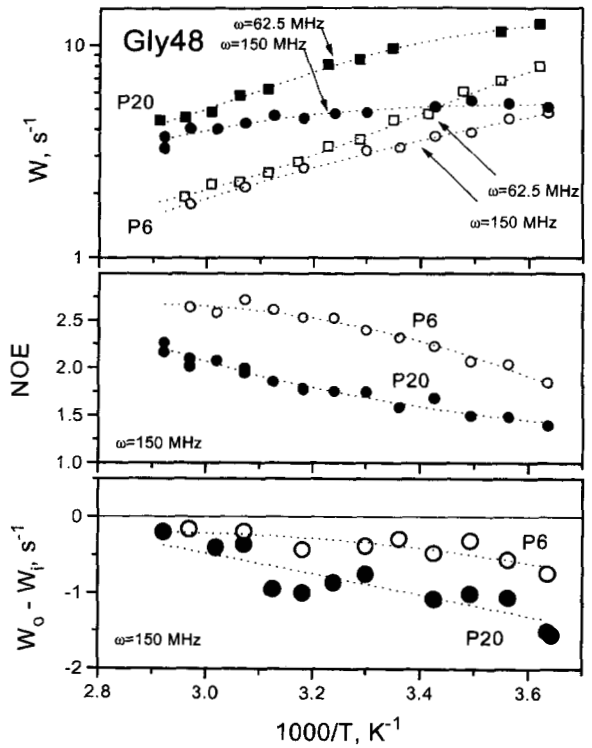

Fig. 3. G48 $^{13}CH_2$ spin-lattice relaxation rates, W (s^{-1}) (top panel), $\{^1H\}$-^{13}C NOE coefficients (middle panel), and cross-correlation spin-lattice relaxation rates, $W_o - W_i$ (s^{-1}) (bottom panel) are shown as a function of the inverse temperature in K^{-1}. Open symbols represent data for P6, and filled symbols represent data for P20. Line fits are the result of polynomial approximations of the temperature dependence of relaxation rates as discussed in the text. Relaxation data are shown for ^{13}C resonance frequencies of 62.5 MHz and for 125 MHz.

additional information for more accurate motional analyses to be described below. Similar relaxation trends were observed for carbons in A43 (Daragan & Mayo, 1996a), T44, and I51. Note also that the temperature dependence in W for G48 (Fig. 3) and for T44 and I51 (Fig. 4) is greater in P5/P6 than it is in P20. For smoothing the non-Arrhenius temperature dependence of relaxation rates, W and NOE data were fit with the polynomial approximation $\log(A + Bx + Cx^2)$, where $x = 1000/T$ (T is the temperature in K). These fits are shown in Figures 3 and 4 as lines through the experimental data points.

The model-free approach parameterized with a single internal rotational correlation time (Equation 1) has been used to analyze relaxation data. Details of the minimization procedure have been described previously (Daragan et al., 1993). Five temperature points were chosen to calculate overall tumbling correlation times (τ_o), internal rotational correlation times (τ_i), and auto- (S_{CH}^2) and cross-correlation (S_{HCH}^2) order parameters for methyl and methylene groups. For this analysis, points were taken from polynomial fits of the temperature dependencies of relaxation data as discussed above.

The overall tumbling correlation times, τ_o, for P5 and P6 range from about 100–200 psec at 323 K to 500–800 psec at 278 K. For P20, these values as expected are larger, but fall within a narrower range: 400–600 psec (323 K) to 1000–1100 psec (278 K). The average activation energy for overall tumbling motions of A43, T44, G48, and I51 C_α carbons in P20 is 4.5 kcal/mol. This value agrees well with data on the collagen IVH1 hexadecapeptide (5

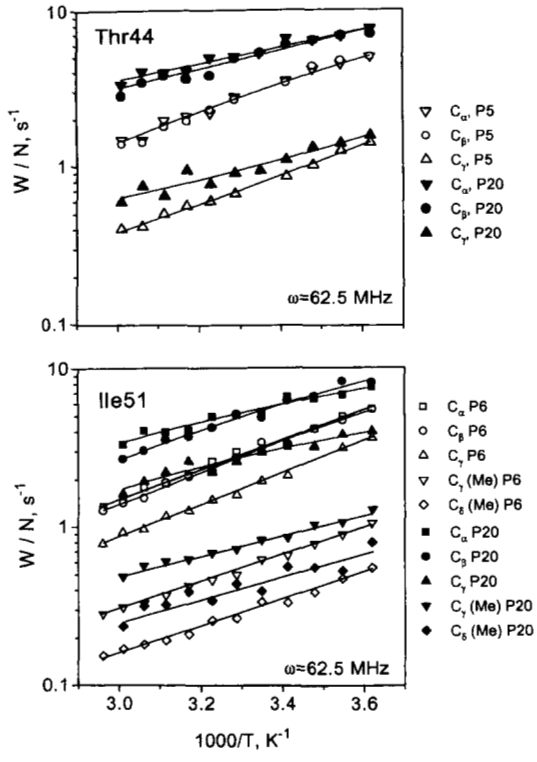

Fig. 4. $^{13}CH_2$ spin-lattice relaxation rates, W (s^{-1}) are shown for T44 (top panel) and for I51 (bottom panel) as a function of the inverse temperature in K^{-1}. Open symbols represent data for the short peptides P5 or P6, and filled symbols represent data for P20. Solid lines are the result of polynomial approximations of the temperature dependence of relaxation rates as discussed in the text. Relaxation data are shown for a ^{13}C resonance frequency of 62.5 MHz. Relaxation rates are given for C_α, C_β, C_γ, and C_δ carbon positions corrected for the number of protons, N, attached to each ^{13}C nucleus. Symbols are defined to the right of each panel.

kcal/mol) (Daragan et al., 1993) and with activation energies for the viscosity of water (4.6 kcal/mol) and for the self- diffusion coefficient of water (5 kcal/mol) (McCall et al., 1959; Tyrrell, 1961).

Backbone C_α motions

The temperature dependencies of C_α order parameters (S^2_α) are shown in Figure 5. In general, for any position in P5, P6, or P20, S^2_α decreases with increasing temperature, indicating—not surprisingly—reduced motional restrictions at higher temperature. Moreover, P20 S^2_α values are mostly larger than or equal to respective order parameters in P5 or P6. In fact, for all but T44, S^2_α values in P20 are larger. The temperature dependence for all C_α order parameters in P20 also fall closer together at any given temperature than they do in P5 and P6. Taken together, these observations suggest that backbone motional restrictions in P20 are a consequence both of increased size of the peptide and of folding. P20 is known to partially fold as a turn/β-sheet at lower temperatures, i.e., 5–10 °C (Ilyina et al., 1994).

For G48 methylene, cross-correlation relaxation data, $W_o - W_i$ (Fig. 3, bottom), are similar to those reported for glycines in the collagen-derived hexadecapeptide IVH1 (Daragan et al., 1993), indicating rather restricted backbone motions. Notice that this appears to be more so for G48 in P20 than in P6; however, G48 motions still remain somewhat restricted even in P6. These values are clearly different at low temperature where P20 is known to fold and become equivalent at high temperature consistent with P20 "unfolding." From analysis of proton-coupled and decoupled ^{13}C relaxation experiments for the G48 CH_2 group, auto- (S^2_{CH}) and cross-correlation (S^2_{HCH}) order parameters were calculated using equation 1. The relationship between S^2_{HCH} and S^2_{CH} has been plotted as a motional restriction map (Fig. 2 in Daragan & Mayo, 1995) in Figure 6. Motional restriction maps provide a means of discriminating among various motional models as indicated by lines and areas on the map as labeled. Actual S^2_{CH} and S^2_{HCH} values for G48 in P6 and P20 are indicated by shaded and solid bars, respectively. The direction for increasing temperature is indicated by the labeled arrow. The widths of these bars correspond to experimental error.

In P6, both G48 S^2_{CH} and S^2_{HCH} order parameters fall on or near the line, which corresponds to a motional model with internal rotations occurring about a single axis with the angle between $C_\alpha H$ bond and axis of rotation, β, being equal to 70.5°. This area of the restriction map (Daragan & Mayo, 1995) corresponds to uncorrelated rotations about ϕ and ψ bonds. Similar data were also obtained for G48 in P20, but only at higher temperatures. This observation is consistent for motions in a less structured peptide. At lower temperatures, G48 order parameters in P20 approach β = 90° indicating that the effective rotational axis has become more perpendicular to the HCH glycine methylene plane. This in turn probably indicates a strong negative correlation for rotational motions about ϕ and ψ bonds at temperatures lower than 10 °C. Such

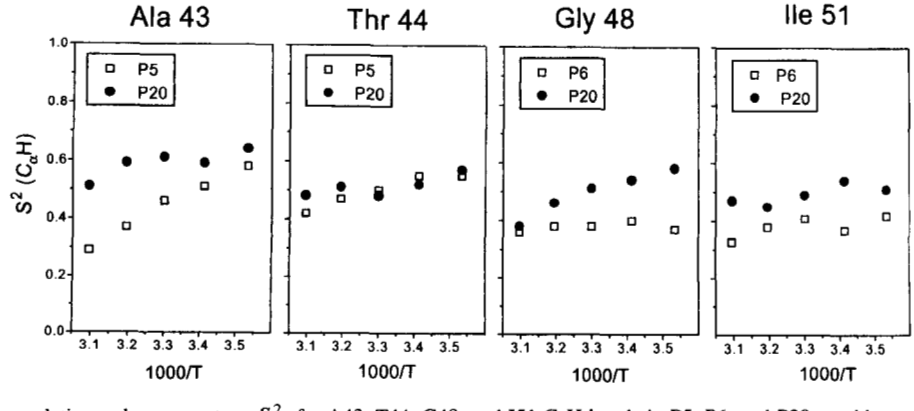

Fig. 5. Auto-correlation order parameters, S^2_α, for A43, T44, G48, and I51 $C_\alpha H$ bonds in P5, P6, and P20 peptides are displayed as a function of the inverse temperature (K^{-1}). S^2_α values are shown for short peptides as open squares and for P20 as filled circles.

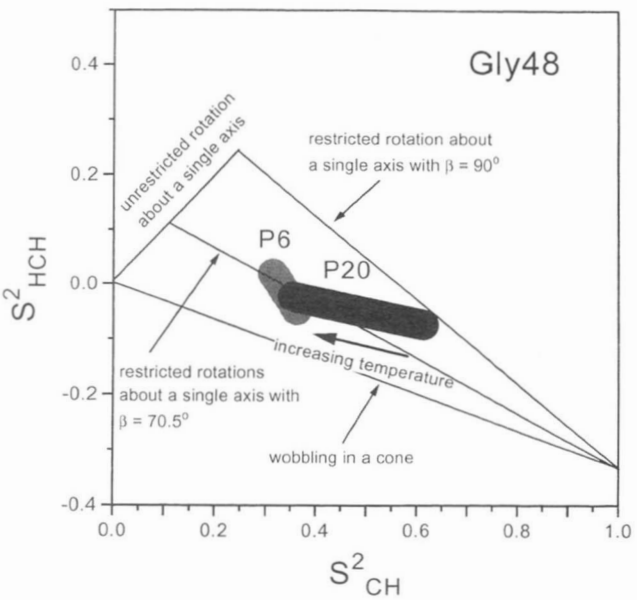

Fig. 6. A motional restriction map is shown for G48 residues in P6 and P20 peptides. The map is generated by plotting the cross-correlation order parameter, S^2_{HCH}, versus the auto-correlation order parameter, S^2_{CH}. Lines on the plot indicate regions where specific types of motions are defined by a given model as labeled in the figure. β is the angle between the CH bond and the axis of rotation. Increasing temperature is indicated by the arrow below data for P20.

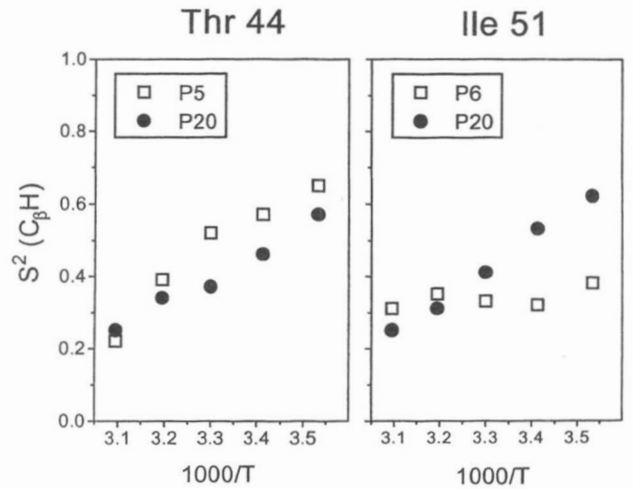

Fig. 7. Auto-correlation order parameters, S^2_α, for T44 and I51 C_βH bonds in P5, P6, and P20 peptides are displayed as a function of the inverse temperature (K^{-1}). S^2_α values are shown for short peptides as open squares and for P20 as filled circles.

rotational motions were observed for the proline $C_\gamma H_2$ group, which undergoes an endo–exo interconversion within the proline ring (Daragan & Mayo, 1995; Mikhailov et al., 1995a). In native PF4 (Mayo et al., 1995), G48 is located in a turn/loop conformation linking two strands of a β-sheet. The general features of this turn/loop structure are preserved in P20 at low temperature (Ilyina et al., 1994). This motional restriction map, therefore, is consistent with the formation of folded structural populations in P20.

The amplitude of rotational restrictions can be estimated by assuming a Gaussian distribution of rotational angles about some equilibrium position. In this case, the auto-correlation order parameter can be written as (Brueschweiler & Wright, 1994):

$$S^2_{CH} = 1 - 3\sin^2\beta_{CH}\sigma^2 \quad (8)$$

where σ is the angular variance in the distribution, and β_{CH} is the angle which the CH bond makes with the axis of rotation. Using equation 8 with $\beta_{CH} = 70.5°$ (higher temperature) and $\beta_{CH} = 90°$ (lower temperature), σ equals 28° and 19.5°, respectively. These amplitudes are typical for backbone rotations in peptides (Daragan & Mayo, 1993) and indicate the degree of rotational restriction imposed in the more folded P20 conformational distribution.

Side-chain motions

Auto-correlation motional order parameters for C_β methines, S^2_β, in T44 and I51 are plotted in Figure 7. S^2_α and S^2_β values vary considerably (compare Fig. 5, 7). Although one might think that backbone motions are more restricted and less temperature dependent than those in side chains, the opposite appears to be true here. While I51 S^2_α and S^2_β values in P6 are essentially identical and show the same temperature behavior, I51 S^2_β values (relative to I51 S^2_α values) in P20 demonstrate a much greater temperature dependence and are larger at lower temperature and smaller at higher temperature, exhibiting a range of 0.25 to 0.65. These data indicate that I51 C_βH can, under certain conditions, exhibit greater motional restriction than its C_αH. Moreover, the enthalpic contribution to motional activation energy is greater for the I51 side chain in P20 than it is in P6. This suggests that mobility is somehow modulated by P20 folding.

For T44, the situation is different. In both P5 and P20, T44 C_βH motions at lower temperatures are similarly restricted, whereas the temperature dependence in S^2_β is greater than it is in S^2_α. This indicates that, independent of P20 folding, the enthalpic contribution to the activation energy for T44 bond rotations is greater for its side-chain C_βH than it is for its backbone C_αH. In the Theory, it was shown that this effect can be explained by considering correlated ϕ, ψ, and χ_1 bond rotations (see Fig. 2). At lower temperatures where $S^2_\beta > S^2_\alpha$, correlations between ϕ and ψ rotations are negative, i.e., $c_{\phi\psi} < 0$, while at higher temperatures bond rotations become uncorrelated.

For the I51 $C_\gamma H_2$ methylene, cross-correlation relaxation data, $W_o - W_i$ (Fig. 8), are also negative as they were for G48, indicating restricted I51 side-chain motions in both P6 and P20. This again is more apparent at lower temperature where folding is evident (Ilyina et al., 1994). At higher temperatures, cross-correlation terms generally become less negative consistent with increased side-chain mobility. Note, however, that S^2_{HCH} remains more negative for the I51 $C_\gamma H_2$ methylene group in P20 than in P6, suggesting possible formation of hydrophobically collapsed species. Figure 9 shows the motional restriction map for the I51 $C_\gamma H_2$ methylene group in P6 and in P20. Compared to the G48 map (Fig. 6), the temperature dependencies of order parameters are not as pronounced, even for P20. Moreover, the motional order parameters for C_βH bond rotations in I51 and in T44 are significantly more sensitive to temperature. In P20, for example, S^2_{CH} for I51 $C_\gamma H_2$ (about 0.22) is considerably less than that for I51 C_βH. In combination with S^2_{HCH} values discussed above, these data indicate that rotations about C_α–C_β bonds are more sensitive to structural changes than are rotations about C_β–C_γ bonds. Both data indicate that for these

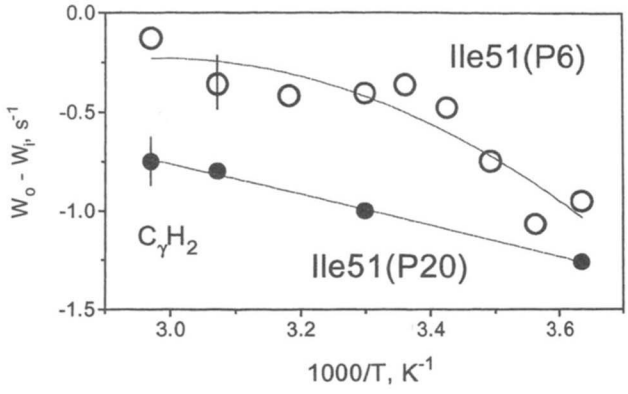

Fig. 8. The differences between the relaxation rates of outer and inner lines, $W_o - W_i$ (s^{-1}), in ^{13}C multiplet spin-lattice relaxation spectra for the I51 $C_\gamma H_2$ methylene group in P6 (open circles) and P20 (filled circles) are shown as a function of the inverse temperature (K^{-1}). Relaxation data were acquired at a ^{13}C resonance frequency of 150 MHz.

peptides, the multiple rotation or wobbling in a cone model for P20 (Daragan & Mayo, 1995) is sufficient to describe the experimental data for rotations of the $C_\gamma H_2$ group. Internal bond rotational restrictions are greater in P20 than they are in P6. This is consistent with observations made for methyl group relaxation data described below.

The temperature dependence of $W_o - W_i$ for ^{13}C in A43, T44, and I51 methyl groups is not as pronounced when compared to methylene motions. Since the motional order parameter for a freely rotating methyl group is limited by theory to a very small value, the internal motional correlation time, τ_i, can be determined fairly accurately. Figure 10 shows the temperature dependence of τ_i for methyl groups in A43 (βH_3), T44 (γH_3), and I51 (γH_3 and δH_3). Equations 1 and 6 were used to analyze $\{^1H\}$-^{13}C NOE and proton-coupled and decoupled ^{13}C relaxation data. τ_i values were calculated by using the model-free approach parameterized with a single internal correlation time. Calculated order parameters S^2_{CH} and S^2_{HCH} were found to be less than 0.1 (data not shown). For I51 $C_\gamma H_3$ and $C_\delta H_3$ groups in P6, the minimization protocol was performed with and without using the cross-correlation spectral density $J_{HCH}(\omega_C)$, and τ_i values were found to be similar. The error in these τ_i calculations is estimated to be less than about 10%. C_β–C_γ bond rotational correlation times were estimated by using Equation 7, and these values were compared to C_β–H bond rotational correlation times determined from C_β relaxation data. These values coincided within 10%, indicating that motions of the C_α–C_β–[$C_\gamma H_3$, $C_\gamma H_2$, H_β] fragment in I51 occur rather symmetrically relative to those of the C_α–C_β bond.

For A43, $C_\beta H_3$, τ_i varies little, if at all, between P5 and P20. In T44 and I51, however, there is a significant difference between methyl group rotations in P20 and in the short peptides. τ_i values are clearly greater for methyl groups in both residues in P20. The difference in fact increases with increasing temperature. The activation energies for internal correlation times range from 2.5 to 4.8 kcal/mol. For P5 and P6, activation energies are all greater than 4 kcal/mol (A43 βH_3: 4.8 kcal/mol; T44 γH_3: 4.4 kcal/mol; I51 γH_3: 4.0 kcal/mol; and I51 δH_3: 4.6 kcal/mol), while for P20 only the A43 activation energy is greater than 4.0 kcal/mol (4.2 kcal/mol). For T44 and I51, methyl group rotational activation energies are less than 3.0 kcal/mol (T44 γH_3: 2.9 kcal/mol; I51 γH_3: 2.5 kcal/mol, and I51 δH_3: 3.0 kcal/mol). In general, therefore, activation energies for methyl group internal rotational correlation times in P20 are less than in the shorter peptides, even though the respective correlation times themselves are greater. Although this seems contradictory, a similar observation was made with short proline-containing peptides in different solvents (Mikhailov et al., 1995a) where it was shown that rotational correlation times in DMSO were much greater than those in water and that the activation energies for these correlation times in DMSO were also greater than in water. The lower activation energies may indicate that these methyl groups are screened from solvent water by inclusion in hydrophobic "pockets" in P20. This is consistent with the presence of populations of folded structure in P20.

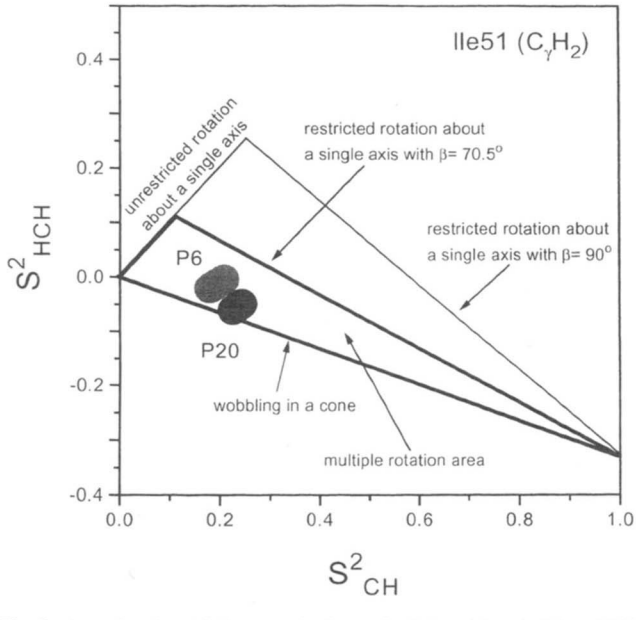

Fig. 9. A motional restriction map is shown for I51 residues in P6 and P20 peptides. The map is generated by plotting the cross-correlation order parameter, S^2_{HCH}, versus the auto-correlation order parameter, S^2_{CH}. Lines on the plot indicate regions where specific types of motions are defined by a given model as labeled in the figure. β is the angle between the CH bond and the axis of rotation. Increasing temperature would be from right to left but, since the temperature effect is so small, this is not indicated.

Conclusions

^{13}C proton-coupled and decoupled NMR relaxation experiments provide unique information concerning peptide internal motions, their restrictions and correlations. Comparison of auto- and cross-correlation order parameters by using a motional restriction map provides an easy way to obtain the direction of the effective rotational axes, as well as the value and sign of rotational correlation coefficients. Even for the same peptide sequence, motional parameters depend on the size of the peptide and its folding capacity. Therefore, for example, formation of the turn/loop at G48 increases $\phi(t)$, $\psi(t)$ rotational correlations. Internal rotations of side chains are also sensitive to peptide structure. These data yield further support for using NMR relaxation to study the intricate details of internal motions in proteins and peptides and the relationship between dynamics and structure.

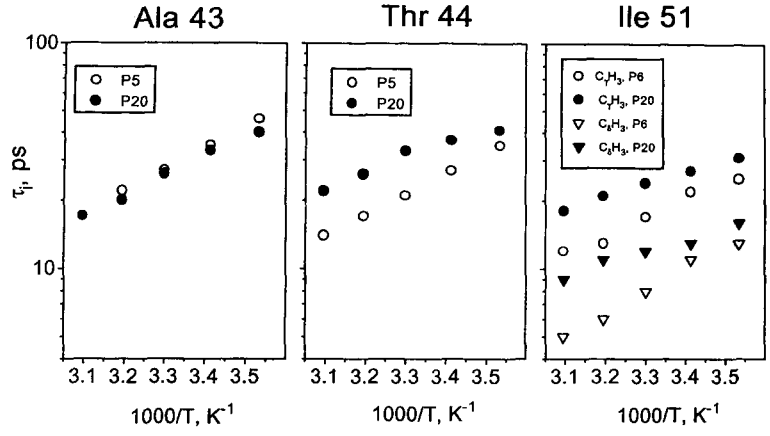

Fig. 10. Internal rotation correlation times, τ_i (ps, picoseconds), of methyl groups in A43, T44, and I51 are shown as a function of the inverse temperature (K^{-1}) for short peptides (P5, P6) as open circles and for P20 as filled circles.

Materials and methods

Six peptides derived from platelet factor-4 (PF4) (Ilyina et al., 1994) and isotopically enriched with ^{13}C-labeled (*) amino acids were synthesized: $I_{42}A^*TLK_{46}$, $I_{42}AT^*LK_{46}$, $N_{47}G^*RKI^*S_{52}$, $T_{38}AQLIATLKNG^*RKI^*SLDLQA_{57}$, $T_{38}AQLIA^*TLKNGRKIS$ $LDLQA_{57}$, and $T_{38}AQLIAT^*LKNGRKISLDLQA_{57}$. Penta-, hexa-, and 20mer peptides are referred to as P5, P6, and P20, respectively (see Fig. 1). The numbering of amino acids in the sequence is the same as in PF4 (Ilyina et al., 1994). Peptides were assembled using Fmoc solid-phase methodology on either a Milligen/Millipore Excell Peptide Synthesizer or on an Applied Biosystems 431A Peptide Synthesizer (Atherton & Sheppard, 1989; Fields & Noble, 1990). Numeration of residues is consistent with the numeration in PF4 (Ilyina et al., 1994). Fmoc-^{13}C alanine, isoleucine, glycine, and threonine were prepared using fully ^{13}C-enriched amino acids (CIL, Cambridge) and Fmoc-OSu (Calbiochem) as described (Fields et al., 1989). Peptide purity was checked by analytical HPLC on a C_{18} Bondclone (Phenomenex) column and fast atom bombardment mass spectrometry. The peptide concentration was determined from the dry weight of freeze-dried samples.

For NMR measurements, freeze-dried samples were dissolved in D_2O. The peptide concentration was less than 10 mg/mL to minimize self-association. The pH was adjusted to pH 6 by adding microliter quantities of NaOD or DCl. Relaxation experiments were performed on Bruker AMX-600 and AM-250 NMR spectrometers operating at ^{13}C frequencies of 150 and 62.5 MHz, respectively. The temperature was varied from 278 K to 348 K.

For increased accuracy, spin-lattice relaxation rates W were determined by using the one-dimensional homonuclear inversion-recovery method with the relaxation delay set at greater than $5 \times T_1$. The number of acquisitions was chosen to give a signal to noise ratio greater than 6. Therefore, the number of transients varied from 32 to 1024. Ten to fifteen times incremented (partially relaxed) spectra were routinely acquired for each relaxation measurement. To reduce errors arising from radio frequency field inhomogeneities, a composite 180° pulse sequence (90°_x–180°_y–90°_x) was used. To reduce contributions from non-exponential relaxation, initial relaxation rates were determined as described by Daragan et al. (1993). $\{^1H\}$-^{13}C NOE measurements were performed by using gated decoupling with a time delay of more than $10 \times T_1$. NOE coefficients (the ratio of irradiated and equilibrium line intensities) represent an average of five separate measurements. Statistical errors for relaxation rates and NOE coefficients were about 5% for P5 and P6 and slightly higher at about 7% for P20.

^{13}C proton-coupled inversion-recovery experiments were performed to obtain cross-correlation spectral densities $J_{HCH}(\omega_C)$. The values of $J_{HCH}(\omega_C)$ for methylene and methyl groups were determined from the difference of the initial slopes of relaxation curves for outer W_o and inner W_i lines in ^{13}C multiplet spectra (Daragan et al., 1993; Daragan & Mayo, 1996a):

$$J_{HCH}(\omega_C) = (5/6)(k^2_{CH})^{-1}\,(W_o - W_i)\ (CH_2\ \text{group})$$
$$J_{HCH}(\omega_C) = (5/12)(k^2_{CH})^{-1}\,(W_o - W_i)\ (CH_3\ \text{group}) \qquad (9)$$

where $k^2_{CH} = h^2\gamma^2_C\gamma^2_H/(4\pi^2 r^6_{CH})$. h is Planck's constant; r_{CH} is the internuclear distance between carbon and its bonded hydrogen; γ_C and γ_H are the magnetogyric ratios for carbon and hydrogen nuclei, respectively. Relaxation curves were analyzed as described previously (Daragan et al., 1993).

For analysis of proton-decoupled ^{13}C relaxation experiments, effects due to dipolar cross-correlations for CH_2 and CH_3 groups were considered. This cross-correlation demonstrates itself as non-exponential behavior in inversion-recovery relaxation curves (Werbelow & Grant, 1977). In order to minimize this contribution, only the initial part of relaxation curves should be considered. Relaxation curves were analyzed using weighted functions (Daragan et al., 1993) so that "tail" points are weighted less. This procedure significantly reduces the error in determining initial slopes of the relaxation curves. Since overall correlation times are more than 50 times greater than internal correlation times, errors from non-exponential behavior in determining initial slopes are less than about 3% (Daragan et al., 1993). Statistical errors were estimated to be less than about 5%. Initial slopes for a CH_N group (N = 1,2,3) can be written as:

$$W = Nk^2_{CH}J^*_{CH}(\omega) \qquad (10)$$

$J^*_{CH}(\omega)$ is defined as the linear combination of spectral densities:

$$J^*_{CH}(\omega) = J^*_{CH}(\omega_C, \omega_H)$$
$$= [J_{CH}(\omega_C - \omega_H) + 3J_{CH}(\omega_C) + 6J_{CH}(\omega_C + \omega_H)]/10. \qquad (11)$$

The equations for the CH_N group (N = 1,2,3) NOE coefficients are given by Werbelow & Grant (1977). For methylene and methyl groups, dipolar cross-correlation terms should be taken into account. Usually, experimental data are not sufficient to calculate all cross-correlation functions for methyl rotations. In this case, these functions can be estimated by using Equations 1 and 6.

Acknowledgments

This work was supported by the National Science Foundation (MCB-9420203) and benefitted from use of the high field NMR facility at the University of Minnesota.

References

Atherton E, Sheppard RC. 1989. *Solid phase peptide synthesis: A practical approach*. Oxford: IRL Press.

Bain AD, Lynden-Bell RM. 1975. The relaxation matrices for AX2 and AX3 nuclear spin systems. *Mol Phys 30*:325–356.

Bremi T, Ernst M, Ernst RR. 1994. Side-chain motion with two degrees of freedom in peptides. An NMR study of phenylalanine side chains in antamanide. *J Phys Chem 98*:9322–9334.

Brüschweiler R, Wright PE. 1994. NMR order parameters of biomolecules: A new analytical representation and application to the Gaussian axial fluctuation model. *J Am Chem Soc 116*:8426–8427.

Canet D. 1989. Construction, evolution and detection of magnetization modes designed for treating longitudinal relaxation at weakly coupled spin 1/2 systems with magnetic equivalence. *Prog NMR Spectrosc 21*:237–291.

Clore GM, Gronenborn AM, eds. 1993. *NMR of Proteins*. Boca Raton: CRC Press.

Clore GM, Szabo A, Bax A, Kay LE, Driscoll PC, Gronenborn AM. 1990. Deviations from the simple two-parameter model-free approach to the interpretation of nitrogen-15 NMR relaxation of proteins. *J Am Chem Soc 112*:4989–4991.

Daragan VA, Khazanovich TN, Stepanyants AU. 1974. Cross-correlation effects in multiplet spectra of ^{13}C. *Chem Phys Lett 26*:89–92.

Daragan VA, Kloczewiak MA, Mayo KH. 1993. ^{13}C-NMR relaxation-derived ψ, ϕ-bond rotational energy barriers and rotational restrictions for glycine ^{13}C-methylenes in a GXX- repeat hexadecapeptide. *Biochemistry 32*:10580–10590.

Daragan VA, Mayo KH. 1993. Tri- and di-glycine backbone rotational dynamics investigated by ^{13}C-NMR multiplet relaxation and molecular dynamics simulations. *Biochemistry 32*:11488–11499.

Daragan VA, Mayo KH. 1995. Using the model free approach to interpret ^{13}C NMR multiplet relaxation data from peptides and proteins. *J Magn Reson 107*:274–278.

Daragan VA, Mayo KH. 1996a. A novel model-free analysis of ^{13}C NMR relaxation of alanine-methyl side-chain motions in peptides. *J Magn Reson 110*:164 – 175.

Daragan VA, Mayo KH. 1996b. Analysis of internally restricted correlated rotations in peptides and proteins using ^{13}C and ^{15}N NMR relaxation data. *J Phys Chem 100*:8378–8388.

Dellwo MJ, Wand AJ. 1989. Model-independent and model-dependent analysis of the global and internal dynamics of cyclosporin A. *J Am Chem Soc 111*:4571–4578.

Fields CG, Fields GB, Noble RL, Cross TA. 1989. Solid phase peptide synthesis of ^{15}N-gramicidins A, B, and C and high performance liguid chromatographic purification. *Int J Peptide Protein Res 33*:298–303.

Fields GB, Noble RL. 1990. Solid phase peptide synthesis utilizing 9-fluorenylmethoxy-carbonyl amino acids. *Int J Peptide Protein Res 35*:161–214.

Grant DM, Mayne CL, Liu F, Xiang TX. 1991. Spin-lattice relaxation of coupled nuclear spins with applications to molecular motion in liquids. *Chem Rev 91*:1591–1624.

Ilyina E, Milius R, Mayo KH. 1994. Synthetic peptides probe folding initiation sites in platelet factor-4: Stable chain reversal found within the hydrophobic sequence LIAT*LKNGR*KISL. *Biochemistry 33*:13436–13444.

Jarvis JA, Craik DJ. 1995. 13C NMR relaxation studies of molecular motion in peptide fragments from human transthyretin. *J Magn Reson B107*:95–106.

Kay LE, Torchia DA. 1991. The effects of dipolar cross correlation on ^{13}C methyl-carbon T1, T2, and NOE measurements in macromolecules. *J Magn Reson 95*:536–547.

Kumar A, Madhu PK. 1996. Cross-correlations in multispin relaxation. *Concepts in Magn Reson 8*:139–163.

Lipari G, Szabo A. 1982a. Model-free approach to the interpretation of NMR relaxation in macromolecules. 1. Theory and range validity. *J Am Chem Soc 104*:4546–4559.

Lipari G, Szabo A. 1982b. Model-free approach to the interpretation of NMR relaxation in macromolecules. 2. Analysis of experimental results. *J Am Chem Soc 104*:4559–4570.

Mayo KH, Roongta V, Ilyina E, Milius R, Barker S, Quinlan C, La Rosa G, Daly TJ. 1995. NMR solution structure of the 32 kD tetrameric platelet factor-4 ELR-motif N-terminal chimer: A symmetric tetramer. *Biochemistry 34*:11399–11409.

McCall W, Douglass DC, Anderson EW. 1959. Diffusion in liquids. *J Chem Phys 31*:1555–1557.

Mikhailov D, Daragan VA, Mayo KH. 1995a. ^{13}C-multiplet NMR relaxation-derived ring puckering and backbone dynamics in proline-containing glycine-based peptides. *Biophys J 68*:1540–1550.

Mikhailov D, Daragan VA, Mayo KH. 1995b. Lysine side-chain dynamics derived from ^{13}C multiplet NMR relaxation studies on di-and tri-peptides. *J Biomol NMR 5*:397–410.

Mispelter J, Lefèvre C, Adjadj É, Quiniou É, Favaudon V. 1995. Internal motions of apo-neocarinostain as studied by ^{13}C NMR methine relaxation at natural abundance. *J Biomol NMR 5*:233–244.

Nicholson LK, Kay LE, Baldisseri DM, Arango J, Young PE, Bax A, Torchia DA. 1992. Dynamics of methyl groups in proteins as studied by proton-detected ^{13}C NMR spectroscopy. Application to the leucine residues of staphylococcal nuclease. *Biochemistry 31*:5253–5263.

Palmer III AG, Rance M, Wright PE. 1991. Intramolecular motions of a zinc finger DNA-binding domain from x fin characterized by proton detected natural abundance ^{13}C heteronuclear NMR spectroscopy. *J Am Chem Soc 113*:4371–4380.

Peng JW, Wagner G. 1992. Mapping of spectral density functions using heteronuclear NMR relaxation measurements. *J Magn Reson 98*:308–332.

Peng JW, Wagner G. 1994. Investigation of protein motions via relaxation measurements. *Methods in Enzymology 239*:563–596.

Peng JW, Wagner G. 1995. Frequency spectrum of NH bonds in Eglin c from spectral density mapping at multiple fields. *Biochemistry 34*:16733–16752.

Stone MJ, Chandrasekhar K, Holmgren A, Wright PE, Dyson HJ. 1993. Comparison of backbone and tryptophan side-chain dynamics of reduced and oxidized *Escherichia coli* thioredoxin using ^{15}N NMR relaxation measurements. *Biochemistry 32*:426–435.

Tyrrell HJV. 1961. *Diffusion and heat flow in liquids*. London: Butterworths.

Vold RL, Vold RR. 1978. NMR relaxation in coupled spin systems. *Progress in NMR Spectroscopy 12*:79–133.

Weaver AJ, Kemple MD, Prendergast FG. 1989. Fluorescence and ^{13}C NMR determination of side-chain and backbone dynamics of synthetic melittin and melittin analogues in isotropic solvents. *Biochemistry 28*:8624–8639.

Werbelow LG, Grant DM. 1977. Intramolecular dipolar relaxation in multi-spin systems. *Adv Magn Reson 9*:189–299.

Zhu L, Kemple MD, Landy SB, Buckley P. 1995. Effect of dipolar cross-correlation on model-free motional parameters obtained from ^{13}C relaxation in AX2 systems. *J Magn Reson B109*:19–30.